Colloid–counterion mixtures: an advanced integral equation

2002 J. Phys.: Condens. Matter 14 9323

(http://iopscience.iop.org/0953-8984/14/40/321)

INSTITUTE OF PHYSICS PUBLISHING JOURNAL OF PHYSICS: CONDENSED MATTER

J. Phys.: Condens. Matter **14** (2002) 9323–9337 PII: S0953-8984(02)36557-3

Colloid–counterion mixtures: an advanced integral equation

Luc Belloni

Direction des Sciences de la Matière, Service de Chimie Moléculaire CEA/SACLAY, 91191–Gif-sur-Yvette Cedex, France

Received 2 May 2002, in final form 30 May 2002
Published 27 September 2002
Online at stacks.iop.org/JPhysCM/14/9323

Abstract

The highly asymmetrical primitive model of colloid–counterion mixtures is solved using the advanced integral equation proposed by Barrat *et al* (Barrat J L, Hansen J P and Pastore G 1988 *Mol. Phys.* **63** 747–67). The approximate bridge functions are expressed in terms of three-particle direct correlation functions, themselves derived from a factorization ansatz and thermodynamical relations. Comparisons with the bare HNC and previous improved closures as well as with recent Monte Carlo simulation data illustrate the efficiency of this equation for the precise determination of the structural and equilibrium properties of highly charged colloidal systems.

(Some figures in this article are in colour only in the electronic version)

1. Introduction

The equilibrium and structural properties of spherical polyelectrolytes such as numerous charged colloidal, micellar or biological solutions are governed by complex electrostatic interactions. The simultaneous presence, required by the electroneutrality condition, of highly charged colloids (polyions) and small oppositely and like-charged ions (counterions and coions), the infinite range of the direct coulombic potentials and the existence of ++ and −− repulsions and +− attractions induce strong and non-additive couplings inside the solution [1]. Within the standard 'DLVO' picture based on a Debye–Hückel analysis, the role of the ions is to form a double layer around each colloid and to screen the repulsive interaction between polyions at large separation [2]. An additional short-range effect concerns the counterions which accumulate in the vicinity of the charged surfaces and reduce the value of the effective macroion charge (ionic condensation) [3]. This mean-field picture, valid at low to intermediate coupling, breaks down at high coulombic coupling, especially in the presence of multivalent counterions. In this regime, ion–ion correlations occur in the medium separating colloids and have a dramatic effect on the effective interaction between approaching polyions and on the stability of the solution. An attraction of pure electrostatic origin may appear in the ion-averaged pair potential, in contradiction with the DLVO view. A correct prediction

and description of this phenomenon requires a careful resolution of the so-called primitive model (PM). The PM neglects the discrete nature of the polar solvent and considers mixtures of charged hard or soft spheres immersed in a continuous dielectric solvent (no electrostatic images, van der Waals and hydration forces). It makes no *a priori* assumptions on the ionic fluid and treats explicitly and on an equal footing large colloids and small ions, as in an asymmetrical electrolyte.

Exact resolutions of the PM of colloidal systems are obtained by numerical Monte Carlo (MC), molecular or Brownian dynamics simulation. Such studies face the intrinsic problems of highly charged systems: the $1/r$ long-range coulombic potential implies the use of time-consuming Ewald summation techniques, the electroneutrality condition multiplies the total number of particles and the ionic condensation of counterions around each colloid requires the use of very small colloidal displacements or time steps. The situation is somewhat simplified in the case of micrometric particles, of size much larger than the screening and condensation lengths. In this particular case, the colloids interact only by pairs and, using the standard Derjaguin transformation, it is sufficient to solve the equivalent problem of two parallel, charged walls separated by a simple electrolyte [4]. Numerous simulation data and theories have shown since the mid-1980s how the Gouy–Chapman, Poisson–Boltzmann pure repulsion between the walls is replaced by a short-range attraction at high coupling [5]. The situation is much more difficult in the nanometric domain, as in micellar or protein systems, where the typical ranges of interaction (Debye screening length, condensation thickness) are not negligible compared with the macroion size and with the mean distance between macroions. This is especially true in *salt-free* solutions, where the single contribution to the ionic strength originates from the counterions and the screening is concentration dependent. In this case, the ion-mediated colloidal interactions become of N-body nature and one cannot avoid simulating the full binary PM at finite colloidal density. The intrinsic difficulties recalled above explain why only moderate charge asymmetries of $1/-12$ to $2/-20$ have been published in the literature since the first MC data in 1982 [6–10], with a few exceptions of $1/-60$ to $3/-60$ in recent years [11]. An alternative to the general PM simulation in bulk is offered by the cell approach, where only two colloids and their ions are simulated in a cell [12]. The colloidal density is implicitly imposed by the cell size and the force felt by both colloids is recorded at different separations. Provided that the separation is much lower than the cell size, this simplified and less complete type of simulation gives information on the colloidal potential of mean force. Both types of simulation, bulk and cell, predict DLVO-like repulsions for monovalent ions and attractions for higher ionic valences. A colloidal aggregation and a destabilization of the solution associated with this attraction are even observed in bulk simulation [13]. Figure 1 shows typical examples of MC snapshots and force–distance curves for $1/-60$ and $2/-60$ systems in the cell geometry. In the monovalent case, the entropy of the numerous free ions guarantees a pure repulsion between colloids. In the divalent case, structures in the two interacting condensation shells appear and strong ion–ion correlations induce attraction at intermediate separation.

Since the PM of bulk colloidal systems is difficult to solve by simulation, there is a need for accurate theories of liquid such as those based on integral equations [14]. The HNC closure, well suited to coulombic systems, is known to predict at finite density and high electrostatic coupling an instability of the PM with respect to liquid–gas phase transition [15, 16]. This phenomenon is illustrated in terms of attractive ion-averaged potential between colloids [1, 17]. Numerous comparisons between HNC results and simulation data, from the restricted PM of a symmetrical electrolyte [18] up to the planar double-layer limit [19], indicate that the general trend of the bulk HNC theory is to overestimate the non-mean-field behaviour and to predict the existence of the attraction at too low coupling. Moreover, the HNC equation is characterized

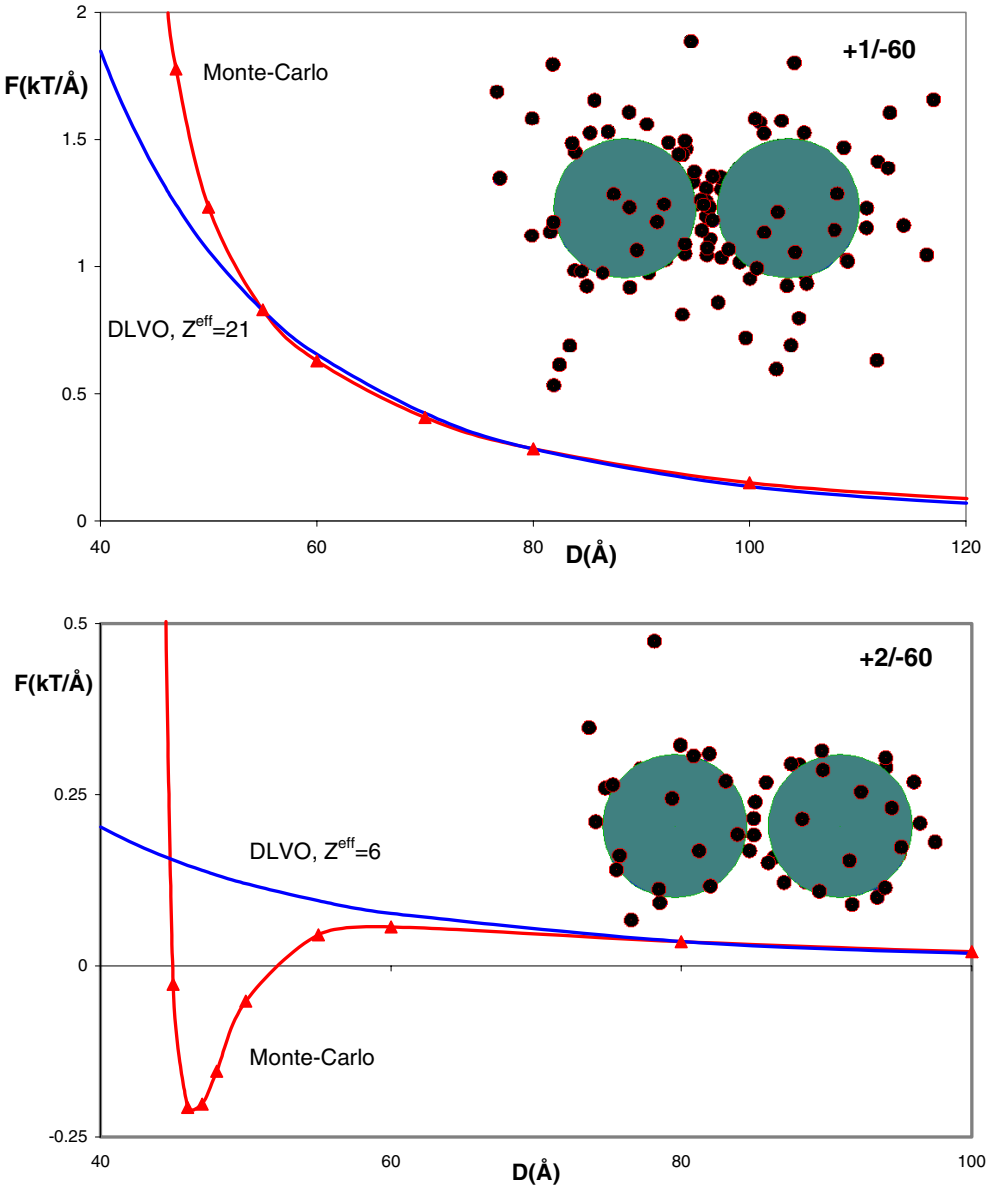

Figure 1. MC force versus separation between two colloids of charge 60 and diameter 40 Å in the cell geometry. Hard-wall cell; no periodic images. $T = 298$ K, $\varepsilon = 78.4$, $\sigma_c = 4$ Å, volume fraction 0.84%. The insets show typical MC snapshots. Monovalent and divalent counterions.

by a thermodynamical inconsistency between the compressibility and virial routes for the pressure [15]. Different directions have been followed in order to improve the bare HNC equation for the asymmetrical PM and to introduce in some approximate ways the so-called bridge function, missing from HNC. Zerah and Hansen (ZH) have proposed a mixed integral equation, which interpolates between HNC at large distances and SMSA (PY for repulsive potential, MSA for attractive potential) at short distances [20]. This phenomenological

equation imposes the thermodynamical self-consistency by construction and modifies the HNC closure in the correct direction [21]. Other attempts consisted in approximating the bridge function by its first diagram in the density expansion [22]. The success of the resulting HNCB equation is restricted to low coupling, as expected. A different class of advanced closure uses the formalism of the multidensity cluster expansion for associating particles and separates the colloid–counterion potential into two parts, a strongly attractive part responsible for the association and a non-associative part [23].

In the present study, we apply the improved integral equation proposed by Barrat, Hansen and Pastore (BHP) [24] to the salt-free, binary PM of colloid–counterion systems. The density functional formalism of inhomogeneous fluids expresses the bridge function in terms of N-body ($N > 2$) direct correlation functions $c^{(N)}$. Using a factorization ansatz for $c^{(3)}$ and the exact relation between $c^{(3)}$ and the density derivative of $c^{(2)}$, BHP have derived a simple and tractable closure, which has proven to be accurate for simple monodisperse fluids [24]. We show in this paper that the BHP integral equation remains powerful in the asymmetrical PM and successfully improves the HNC data in terms of self-consistency and when compared with simulation data.

2. Theory

The binary system is composed of polyions (p) of number charge Z_p and density ρ_p and counterion (c)(Z_c, ρ_c). The electroneutrality condition imposes $Z_p\rho_p + Z_c\rho_c = 0$. $\rho = \rho_p+\rho_c$ is the total density. The pair potential $v_{ij}(r)$ between species i and j contains the long-range $1/r$ coulombic contribution and the short-range, hard or soft, repulsion:

$$\beta v_{ij}(r) = \beta v_{ij}^{SR}(r) + Z_i Z_j L_B/r; \tag{1}$$

$\beta = 1/(kT)$, $L_B = e^2/(4\pi\varepsilon_0\varepsilon kT)$ is the Bjerrum length and ε is the dielectric constant of the solvent. For hard-sphere particles of diameter σ_i,

$$\beta v_{ij}^{SR}(r) = \begin{cases} +\infty; & r < \sigma_{ij} = (\sigma_i + \sigma_j)/2 \\ 0; & r > \sigma_{ij}. \end{cases} \tag{2}$$

The calculation of the pair distribution functions $g_{ij}(r)$ starts with the multi-component Ornstein–Zernike (OZ) equation which relates total $h_{ij} = g_{ij} - 1$ and direct c_{ij} pair correlation functions [14]:

$$h_{ij}(r_{12}) = c_{ij}(r_{12}) + \sum_k \rho_k \int h_{ik}(r_{13}) c_{kj}(r_{32})\, \mathrm{d}\boldsymbol{r}_3. \tag{3}$$

The formally exact closures read

$$g_{ij} = \exp[-\beta v_{ij} + h_{ij} - c_{ij} + b_{ij}] \tag{4}$$

where the b_{ij} represent the bridge functions. The HNC approximation consists of neglecting these functions, $b_{ij} = 0$. The first renormalized bridge diagram reads [14]

$$b_{ij}(r_{12}) \approx \tfrac{1}{2} \sum_{k,l} \rho_k \rho_l \iint h_{ik}(r_{13}) h_{il}(r_{14}) h_{jk}(r_{23}) h_{jl}(r_{24}) h_{kl}(r_{34})\, \mathrm{d}\boldsymbol{r}_3\, \mathrm{d}\boldsymbol{r}_4. \tag{5}$$

This approximation for b_{ij} defines the HNCB closure [22].

A better approximation for the bridge functions, valid on a wider range of coupling, involves the three-body direct correlation functions [24, 25]:

$$b_{ij}(r_{12}) \approx \tfrac{1}{2} \sum_{k,l} \rho_k \rho_l \iint h_{ik}(r_{13}) h_{il}(r_{14}) c_{jkl}^{(3)}(\boldsymbol{r}_{23}, \boldsymbol{r}_{24})\, \mathrm{d}\boldsymbol{r}_3\, \mathrm{d}\boldsymbol{r}_4. \tag{6}$$

This expression is the first term in a systematic expansion within the density functional formalism of inhomogeneous fluids. Exact relations relate the partial integrals of the $c^{(3)}_{ijk}$ to the partial density derivatives of c_{ij}:

$$\int c^{(3)}_{ijk}(\boldsymbol{r}_{12}, \boldsymbol{r}_{13})\,\mathrm{d}\boldsymbol{r}_3 = \frac{\partial c_{ij}(r_{12})}{\partial \rho_k}. \tag{7}$$

In order to obtain an accurate but tractable theory, BHP have proposed to factorize the three-body functions $c^{(3)}_{ijk}$ in [24]:

$$c^{(3)}_{ijk}(\boldsymbol{r}_{12}, \boldsymbol{r}_{13}) = t_{ij,k}(r_{12})t_{ik,j}(r_{13})t_{jk,i}(r_{23}). \tag{8}$$

This approximate factorization ansatz verifies required symmetry relations. The new functions $t_{ij,k}(r)$ are derived from the relations (7):

$$t_{ij,k}(r_{12}) \int t_{ik,j}(r_{13})t_{jk,i}(r_{23})\,\mathrm{d}\boldsymbol{r}_3 = \frac{\partial c_{ij}(r_{12})}{\partial \rho_k}. \tag{9}$$

The new bridge functions become

$$b_{ij}(r_{12}) \approx \tfrac{1}{2}\sum_{k,l} \rho_k \rho_l \iint h_{ik}(r_{13})h_{il}(r_{14})t_{jk,l}(r_{23})t_{jl,k}(r_{24})t_{kl,j}(r_{34})\,\mathrm{d}\boldsymbol{r}_3\,\mathrm{d}\boldsymbol{r}_4. \tag{10}$$

Equations (4) and (10) with relations (9) define the BHP closure. With the simple approximation $t_{ij,k} = h_{ij}$ asymptotically valid at zero density, equation (10) coincides with (5) and one recovers the HNCB closure.

For binary systems, the three pair distribution functions g_{pp}, g_{pc} and g_{cc} require the calculation of six functions $t_{ij,k}$. Note the *a priori* difference between $t_{ij,1}$ and $t_{ij,2}$. Equations (9) involving $t_{11,1}$ and $t_{22,2}$ are independent, those involving $t_{11,2}$, $t_{12,1}$ on one side and $t_{22,1}$, $t_{12,2}$ on the other side are coupled two by two [24].

The complete BHP resolution for a given set of pair potentials is the following.

(i) Starting from imposed functions b_{ij}, the equations (4) with the OZ equations (3) (expressed in Fourier space) are solved using the standard iterative process [15, 21]. At this stage, this is equivalent to solving HNC with the potentials $v_{ij} - kTb_{ij}$. Extensive use is made of the powerful Newton–Raphson techniques proposed by Zerah [26].

(ii) The partial derivatives $\partial c_{ij}/\partial \rho_k$ $(i, j = p, c)$ are obtained by explicitly differentiating the previous cycle with respect to the density ρ_k. The technique detailed in appendix A is equivalent to that used for the numerical derivation of the virial compressibility [21].

(iii) The six functions $t_{ij,k}$ are calculating by solving the six equations (9) using steepest-descent and conjugate gradient methods (appendix B).

(iv) The sixfold integrals in the bridge function expressions (10) are routinely reduced to sums of double integrals by Legendre polynomial expansions [27].

(v) With the new estimates of b_{ij}, the cycle is repeated again at stage (i). The process is iterated until convergence is reached.

A few remarks on this iterative resolution: in general, the first iteration is started with $b_{ij} = 0$ (HNC solution). In cases where HNC has no solution for the state under study, one starts with the bridge functions of a close previously solved state. During step (ii), the dependence of b_{ij} on ρ_k is neglected for simplicity. The calculation of the $t_{ij,k}$ during step (iii) is the most sensitive part in the resolution. The structure of equations (9) induces intrinsic problems of convergence discussed in appendix B. Contrary to equation (5) and, less obviously, to equation (6), the BHP approximation (10) for b_{ij} loses its required symmetry in ij. This means that the calculation of b_{pc} and b_{cp} in step (iv) gives two different bridge functions,

which is not satisfactory. Thus, the symmetry has been imposed by choosing $(b_{pc} + b_{cp})/2$ for the cross bridge function. Lastly, the convergence is usually obtained with one or two iterations. In some particular cases where the starting function b_{ij} is far from the final one, the resolution may converge more slowly with some oscillations. Interpolation of successive functions speeds up the convergence.

Once the convergence is reached, the pressure P as well as the normalized isothermal compressibility $\chi = \partial\rho/\partial(\beta P)$ are derived from the virial equation [14]. In order to check the thermodynamical consistency of the theory, this value χ_v of χ is compared with the value χ_c deduced from the compressibility equation which involves the partial structure factors $S_{ij}(q)$ at the origin $q = 0\,(Z \equiv |Z_p/Z_c|)$:

$$\chi = (Z+1)S_{pp}(0) = (Z+1)/ZS_{cc}(0). \tag{11}$$

Within the BHP approximation for the $c^{(3)}$ and b functions, an explicit expression for the excess chemical potentials in terms of the pair correlation functions is conserved [28]:

$$\beta\mu_i^{exc} = \sum_j \rho_j \int [h_{ij}(r)(h_{ij}(r) - c_{ij}(r))/2 - c_{ij}(r)]\,\mathrm{d}\boldsymbol{r} + \sum_j \rho_j \int b_{ij}(r)[1 + 2/3h_{ij}(r)]\,\mathrm{d}\boldsymbol{r}. \tag{12}$$

The colloid pair correlations described by $g_{pp}(r)$ and $S_{pp}(q)$ can be advantageously illustrated in terms of the *effective*, ion-averaged pair potential $v_{pp}^{eff}(r)$ [13, 17, 29]. By definition, this potential leads, within a one-component approach, to the same *pair* colloidal correlations as within the PM, at identical temperature and colloidal density [30]. The extraction of $v_{pp}^{eff}(r)$ requires the inversion of the integral equation problem in the one-component model:

$$\beta v_{pp}^{eff} = h_{pp} - c_{pp}^{eff} - \ln g_{pp} + b_{pp}^{eff}. \tag{13}$$

The function c_{pp}^{eff} is easily deduced from S_{pp} through the one-component OZ equation expressed in Fourier space. In principle, the approximation chosen for the one-component bridge function b_{pp}^{eff} must be consistent with that previously used in the binary PM. In the HNC approximation, $b_{pp}^{eff} = 0$. In the HNCB approximation, $b_{pp}^{eff}(r)$ is given by the unique diagram $i = j = k = l \equiv p$ in (5). Within the BHP approximation, b_{pp}^{eff} is not known *a priori* and must be determined by iteration: from a first estimate, the effective potential is derived with (13). The one-component BHP equation is then solved for that potential in order to deduce the t_{pp}^{eff} function and the new estimate of b_{pp}^{eff}. Two iterations are generally sufficient.

3. Results

We first investigate the reference system in the micellar regime, $T = 298$ K, $\varepsilon = 78$, $Z_i = +1/-40$, $\sigma_i = 5/50$ Å, $\rho_i = 0.1/0.0025$ M (≈10% in volume fraction), previously studied extensively with HNC and ZH [15, 21]. Figures 2–4 present the BHP g_{ij}, $t_{ij,k}$ and b_{ij} functions, respectively. The pair distribution functions reveal a classical behaviour in such a colloid–counterion system: the strong coulombic attraction between oppositely charged objects induces an ionic accumulation or condensation in the vicinity of the polyions, seen in the peak of g_{pc} near contact and in the characteristic shape of g_{cc}. The g_{pp} curve is *a priori* consistent with a three-dimensional liquid order and a purely repulsive effective interaction between colloids. The $t_{ij,k}$ functions present much more complex structures than their asymptotic values h_{ij}. Moreover, $t_{ij,p}$ differs from $t_{ij,c}$ for the three pairs i, j. The resulting bridge functions take negative values, which means that the BHP theory, compared with HNC,

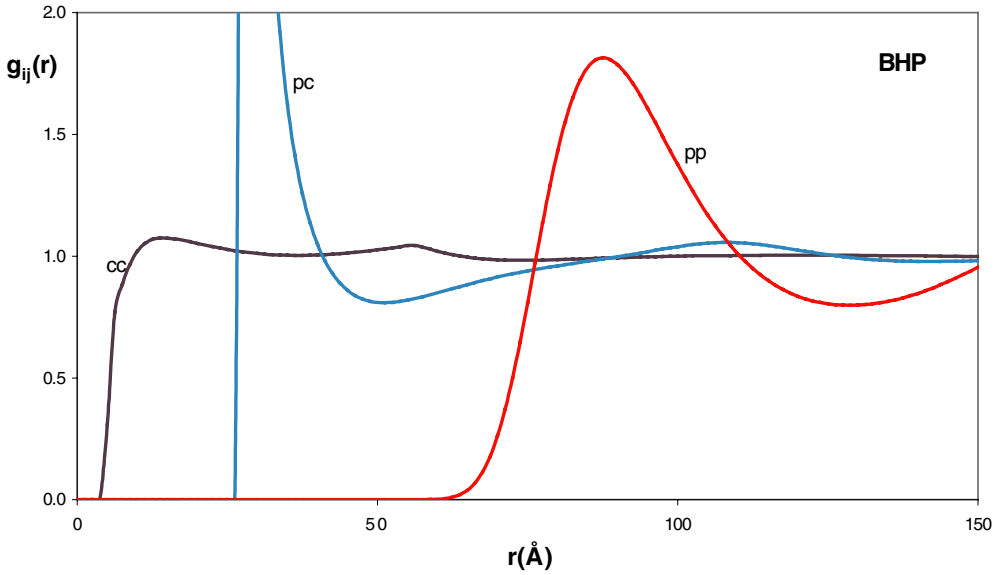

Figure 2. Pair distribution functions $g_{ij}(r)$ for the $+1/-40$ system. $T = 298$ K, $\varepsilon = 78$, $\sigma_i = 5/50$ Å, $\rho_p = 0.0025$ M. BHP equation.

should weaken the ionic condensation and ion–ion correlations inside the condensation shell and strengthen the effective colloidal repulsion. As said in the introduction, this is the needed and expected trend to improve the HNC data. This is confirmed in figures 4–7, where the HNC, HNCB, ZH and BHP results are compared for $b_{ij}(r)$, $g_{ij}(r)$, $S_{ij}(q)$ and $v_{pp}^{eff}(r)$, respectively. The corresponding thermodynamical quantities are given in table 1. The particular HNC behaviour is clearly identified: the strong ionic condensation and the absence of the polyion–polyion bridge function induces a somewhat weak effective repulsion at short distance and the presence of an effective attraction at intermediate distance [17]. The high values $S_{ij}(0)$ of the partial structure factors at $q = 0$ mean a severe inconsistency between compressibility and virial routes for the pressure [15]. The first bridge diagrams (5) of the HNCB approximation, shown in figure 4 for comparison, are much smaller than the BHP ones, especially for b_{pp}, and bring minor corrections to HNC. The attractive contribution has disappeared in the HNCB effective potential but the disagreement between χ_c and χ_v remains. On the other hand, the BHP curves present a stronger three-dimensional liquid order among the colloids (g_{pp} in figure 5) with a peak higher and localized at larger distance than for HNC or HNCB. Equivalently, the effective potential presents an enhanced repulsion in figure 7 and the $S_{ij}(0)$ values are lower in figure 6. The resulting BHP thermodynamical consistency in table 1 is much better and almost perfect when the density dependence of the bridge function is partially taken into account (see appendix A). Lastly, the phenomenological ZH approximation which imposes self-consistency by adjusting the parameter of mixing between HNC, PY, MSA closures (ZHb version [21]) presents results surprisingly close to the BHP advanced theory.

The next systems, $T = 298$ K, $\varepsilon = 78.4$, $Z_p = -20$, $\sigma_i = 4/30$ Å, again in the nanometric regime, have been studied by different groups with MC simulation for two colloidal densities, $\rho_p = 0.01$ and 0.02 M (≈8.5 and 17% in volume fraction) and two counterion valences $Z_c = +1$ and +2 [10]. Figures 8 and 9 display the polyion–polyion pair distribution functions for the monovalent and divalent cases, respectively. For the $+1/-20$ concentrated case, the

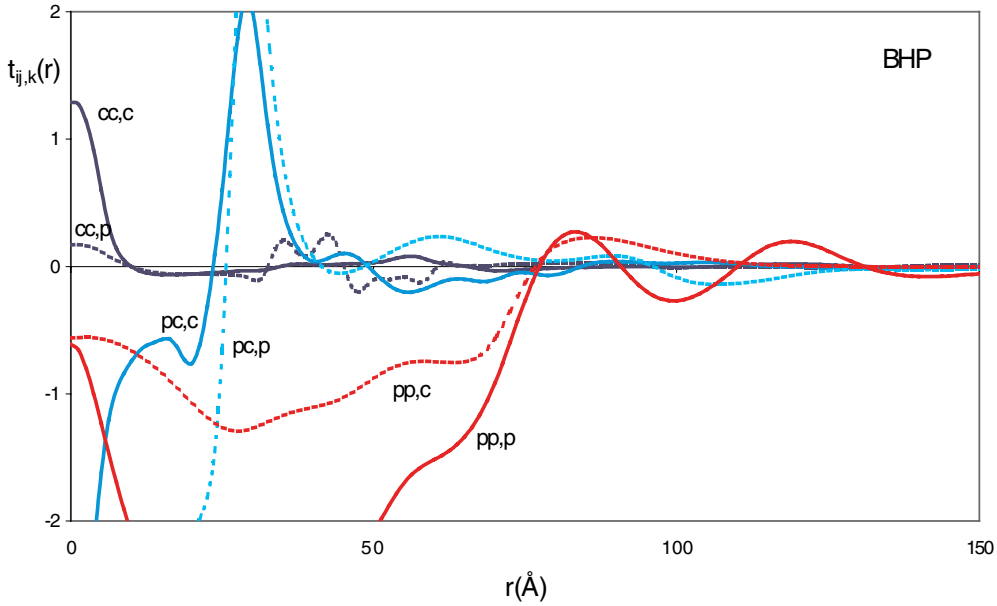

Figure 3. BHP functions $t_{ij,k}(r)$. The same system as for figure 2.

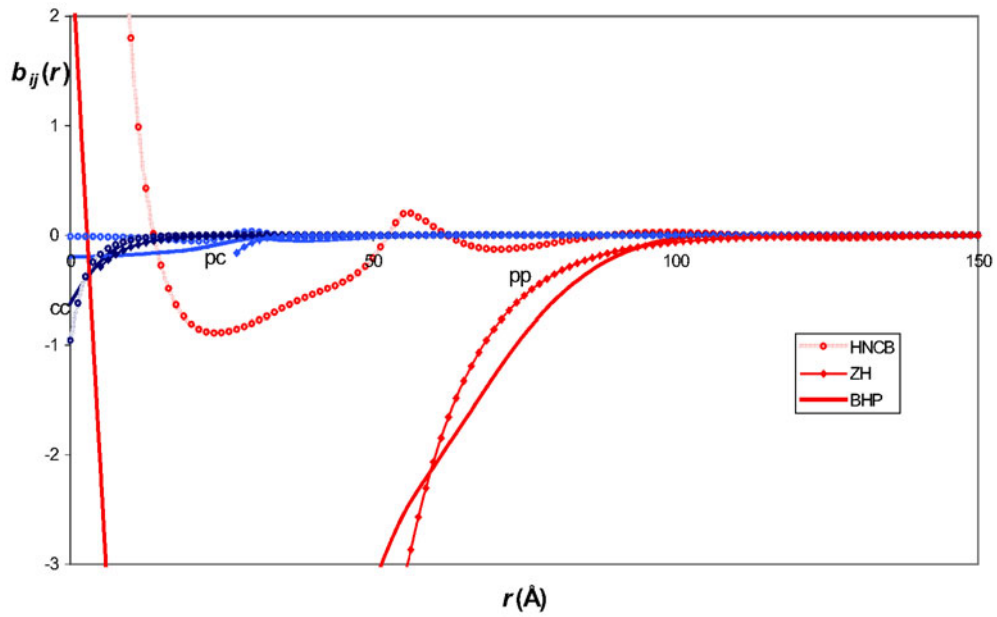

Figure 4. Bridge functions $b_{ij}(r)$. The same system as for figure 2. HNCB, ZH and BHP equations.

peak height and position have been improved going from HNC to BHP, as compared with the MC data. The HNC self-inconsistency ($\chi_c = 0.69$, $\chi_v = 0.96$) is corrected with BHP ($\chi_c = 0.94$, $\chi_v = 0.80/0.90$). A slight shoulder appears on the right of the main peak of $g_{pp}(r)$, which becomes more apparent in the effective potential curve $v_{pp}^{eff}(r)$ (inset in figure

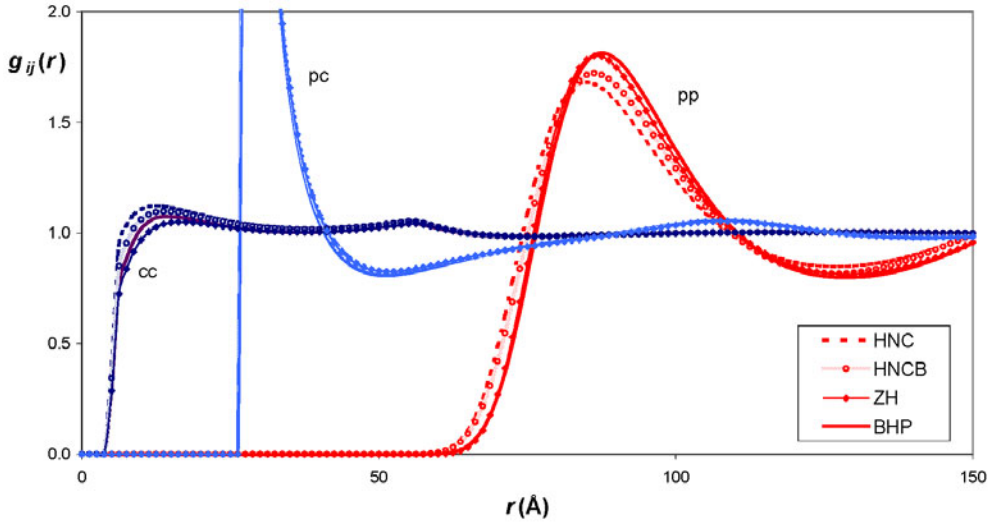

Figure 5. Pair distribution functions $g_{ij}(r)$. The same system as for figure 2. HNC, HNCB, ZH and BHP equations.

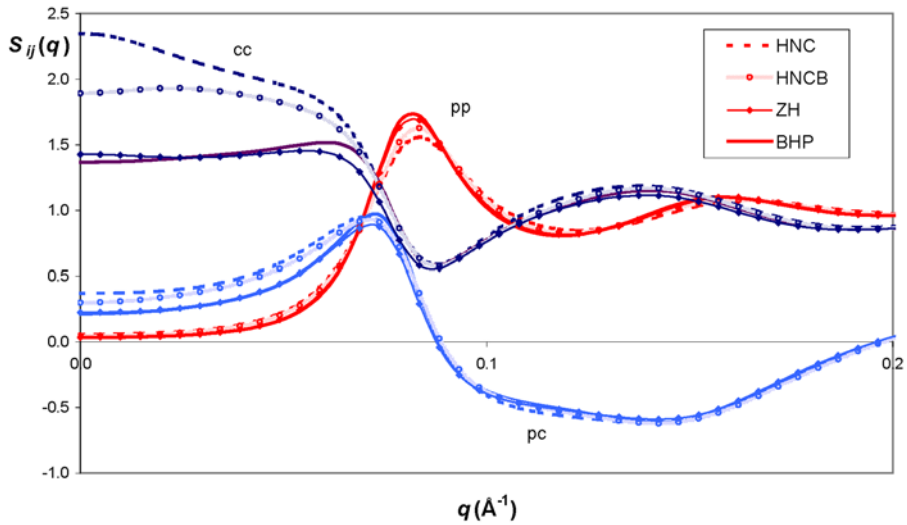

Figure 6. Partial structure factors $S_{ij}(q)$. The same system as for figure 2. HNC, HNCB, ZH and BHP equations.

8). This is due to a small positive peak in the bridge function $b_{pp}(r)$ at these distances. Due to the spreading in the MC data[1], no definite conclusion can be made about the relevance of this BHP shoulder. For the $+1/-20$ dilute case, the HNC equation has no solution (the system lies inside the HNC liquid–gas region), while the BHP equation presents a fair agreement with MC ($\chi_c = 1.75$, $\chi_v = 1.34/1.50$). Note that the present colloidal system with charge asymmetry $+1/-20$ is counter-intuitively more coupled than the $+1/-40$ case investigated before. This is

[1] The different papers listed in [10] do not present exactly the same MC $g_{pp}(r)$ curves. The data given in figures 8, 9 are those of Hribar and Vlachy.

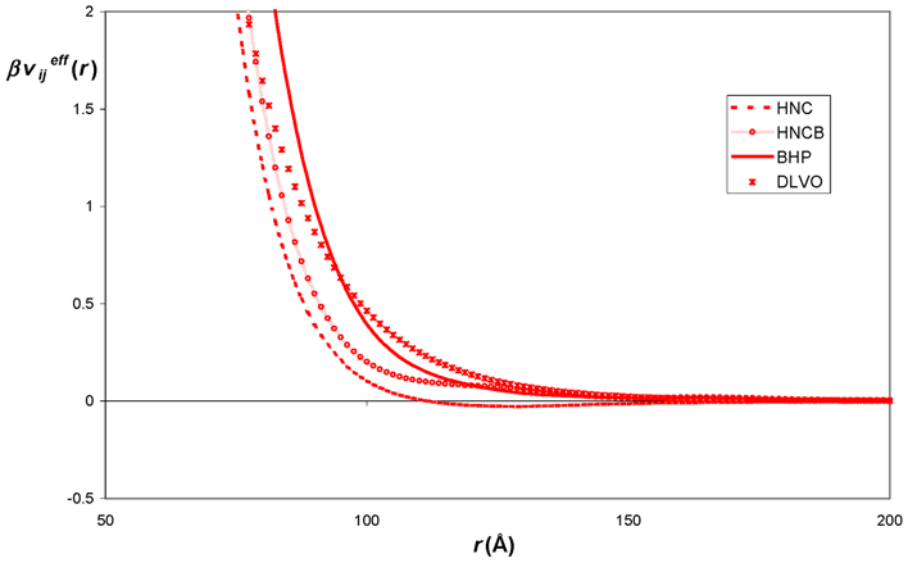

Figure 7. Effective, ion-mediated colloid–colloid potential $v_{pp}^{eff}(r)$. The same system as for figure 2. HNC, HNCB and BHP equations. The effective potential is extracted using the same closures within the one-component model.

Table 1. Normalized compressibility χ from compressibility 'c' and virial 'v' routes, osmotic coefficient $\beta P/\rho$, polyion–counterion pair distribution function at contact g_{pc}^{max}, post-condensation, effective charge Z_p^{eff} and excess chemical potentials $\beta\mu_i^{exc}$.

Equation	χ_c	χ_v	$\beta P/\rho$	g_{pc}^{max}	$Z_p^{eff(c)}$	$\beta\mu_c^{exc}$	$\beta\mu_p^{exc}$
HNC	2.41	1.26	0.602	8.72	−20.1	0.604	−201.7
HNCB	1.94	1.25/1.28[a]	0.597	8.70	−19.7	0.598	−201.8
ZH[b]	1.45	1.45	0.475	7.65	−21.3		
BHP	1.40	1.30/1.40[a]	0.570	8.46	−20.4	0.601	−203

[a] The two values for χ_v are calculated with $\partial b_{ij}/\partial\log(\rho) = 0$ and $2b_{ij}$, respectively (see appendix A).
[b] The version of ZH chosen here is the version ZHb of [21] ($\alpha_{ij} = cte = 0.075$ Å^{-1}).
[c] The value of the effective charge is extracted from the colloid– counterion profile according to [15].

due to the fact that the colloid is smaller (30 instead of 50 Å in diameter), leading to stronger ion–ion correlations. In the presence of divalent counterions, both HNC and BHP correctly reproduce the MC pair colloidal correlations for the concentrated system. The shape and peak position of $g_{pp}(r)$ in figure 9 are completely different from their counterparts in figure 8. The effective potential mediated by the counterions now presents a clear attraction at intermediate separation (inset in figure 9). This behaviour is emphasized for the dilute $+2/-20$ system. Neither HNC nor BHP have a solution. Starting from the dilute $+1/-20$ case and continuously increasing the ionic valence, the BHP equation loses its solution around $Z_c = 1.9$. This means that the dilute $+2/-20$ lies just inside the BHP two-phase region. In the same way, the MC data present a very unusual g_{pp} function, which means that some kind of phase transition happens near this state.

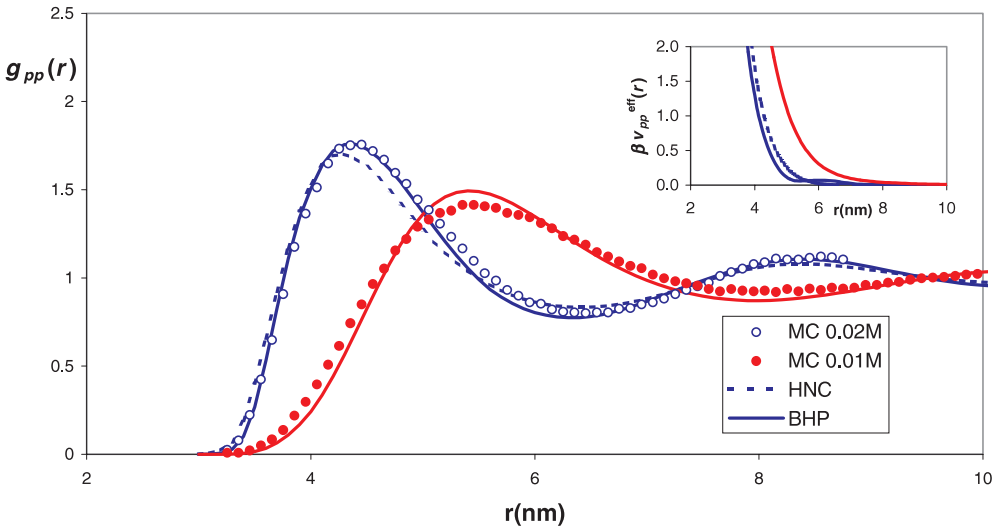

Figure 8. Polyion–polyion pair distribution functions $g_{pp}(r)$ for the $+1/-20$ system. $T = 298$ K, $\varepsilon = 78.4$, $\sigma_i = 4/30$ Å, $\rho_p = 0.01$ and 0.02 M. MC data [10]. HNC and BHP equations. Inset: effective potential $v_{pp}^{eff}(r)$ extracted using the same closures within the one-component model.

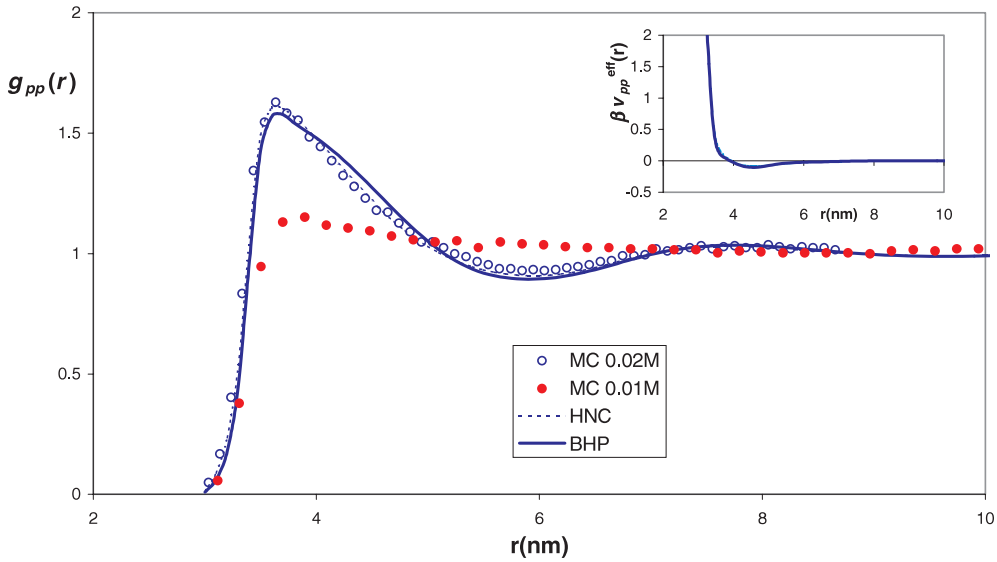

Figure 9. The same as for figure 8 for the $+2/-20$ system.

4. Conclusion

The BHP integral equation proposed by Barrat, Hansen and Pastore greatly improves the HNC results for the PM of colloid–counterion mixtures. The BHP bridge function differs considerably from the first bridge diagram. The liquid–gas domain in the phase diagram, related to an ion-averaged effective *attraction* between colloids, is shifted to higher coulombic coupling. The main formal advantage of this advanced closure is that its bridge function

approximation has been derived from a fundamental and systematic analysis involving high-order direct correlation functions, valid for any interaction potential. This should be compared with phenomenological equations such as ZH or 'reference' or 'modified' HNC, which mix simple closures with one or many adjustable parameters or make *a priori* assumptions about a possible universality of the bridge functions. For the highly asymmetrical PM, the BHP analysis should be continued following different directions.

(i) The determination of the $t_{ij,k}$ functions is the crucial step in the numerical process. Alternative 'easier' choices for the BHP prescription should be derived and tested.
(ii) During the calculation of the $\partial c_{ij}/\partial\rho_k$ derivatives, the density dependence of the bridge functions, ignored for the moment, should be investigated.
(iii) Lastly, the study of higher coulombic coupling should allow us to determine the precise location of the phase transition in the phase diagram.

Work on these points is in progress.

Appendix A

A.1. Determination of the $\partial c_{ij}/\partial\rho_k$ derivatives

The derivative of the OZ equation (3) with respect to the density ρ_k gives

$$\frac{\partial h_{ij}}{\partial\rho_k} = \frac{\partial c_{ij}}{\partial\rho_k} + h_{ik} \otimes c_{kj} + \sum_l \rho_l \left(\frac{\partial h_{il}}{\partial\rho_k} \otimes c_{lj} + h_{il} \otimes \frac{\partial c_{lj}}{\partial\rho_k} \right) \tag{A.1}$$

where the symbol $\otimes$ represents a convolution product. If we denote by $\hat{h}_{ij}(q)$ the Fourier transform (FT) of $h_{ij}(r)$ normalized by the density factor $(\rho_i\rho_j)^{1/2}$ and by $\hat{H}^{(k)}_{ij}(q)$ the similarly normalized FT of $H^{(k)}_{ij}(r) = \partial h_{ij}(r)/\partial\log(\rho_k)$ (with equivalent definitions for c_{ij}), the OZ equations (3) and the equations (A.1) become in Fourier space and matricial notation, respectively

$$\boldsymbol{S} = (\mathbf{1} + \hat{\boldsymbol{h}}) = (\mathbf{1} - \hat{\boldsymbol{c}})^{-\mathbf{1}} \tag{A.2}$$

$$\hat{\boldsymbol{H}}^{(k)} = \boldsymbol{S}\hat{\boldsymbol{C}}^{(k)}\boldsymbol{S} + \boldsymbol{u}^{(k)}\boldsymbol{S}. \tag{A.3}$$

The matrix $\boldsymbol{S}$ is composed of the partial structure factors $S_{ij} = \delta_{ij} + \hat{h}_{ij}$. The element ij of the matrix $\boldsymbol{u}^{(k)}$ is $\hat{h}_{ik}\hat{c}_{kj}$. It should be noted that the infinite range of the coulombic potentials, or equivalently the fact that it is impossible to vary the polyion and counterion densities independently, induces a q^{-2} divergence in the matrices $\hat{\boldsymbol{c}}$, $\hat{\boldsymbol{C}}^{(k)}$ and $\hat{\boldsymbol{u}}^{(k)}$ at the origin $q = 0$. As usual, this divergence disappears in the product of these functions with $\boldsymbol{S}$ thanks to the electroneutrality condition. For example, the element ij of the product $\boldsymbol{u}^{(k)}\boldsymbol{S}$ is $\hat{h}_{ik}\hat{h}_{kj}$.

The derivative of the integral equation (4) reads

$$H^{(k)}_{ij} = g_{ij}(H^{(k)}_{ij} - C^{(k)}_{ij} + B^{(k)}_{ij}). \tag{A.4}$$

Since b_{ij} is a given function during this step, no information is known about its density partial derivatives. For simplicity, we neglect this higher-order effect, $B^{(k)}_{ij} = 0$.

The linear system (A.3), (A.4) is solved by iteration using the same Newton–Raphson techniques as for the integral equation resolution [21]. The convergence is obtained in fewer than ten iterations. This procedure, repeated for $k = p$ and c, gives all desired functions $C^{(k)}_{ij} = \partial c_{ij}/\partial\log(\rho_k)$.

When one needs to calculate the derivatives of the correlation functions with respect to the *total* density ρ, at constant composition, the superscript $^{(k)}$ is dropped from equations (A.3)

and (A.4) and the matrix $\boldsymbol{uS}$ becomes $\hat{\boldsymbol{h}}^{\boldsymbol{2}}$. The functions H_{ij}, when introduced into the derivative of the virial equation, give the virial compressibility $\chi_v = \partial\rho/\partial(\beta P)$. In this case, it is possible to investigate the effect of the ρ-dependence of the bridge functions by comparing the value of χ_v obtained with $B_{ij} = 0$ with that obtained with $B_{ij} = 2b_{ij}$ (quadratic dependence on ρ).

Appendix B

B.1. Determination of the function $t_{11,1}$ (same procedure for $t_{22,2}$)

If we denote $\partial c_{11}(r)/\partial\rho_1$ by $C_1(r)$ and $t_{11,1}(r)$ by $T_1(r)$, the first equation (9) becomes

$$T_1(T_1 \otimes T_1) = C_1. \tag{B.1}$$

The numerical problem is here identical to that faced in one-component systems [24]. The idea is to minimize by iterations the functional

$$f[T_1] = \tfrac{1}{2}\int [D_1(r)]^2\,\mathrm{d}\boldsymbol{r} \equiv \tfrac{1}{2}\int [C_1 - T_1(T_1 \otimes T_1)]^2\,\mathrm{d}\boldsymbol{r} \tag{B.2}$$

with respect to $T_1(r)$.

In the steepest-descent method, the $(n+1)$th iteration estimate is chosen in the direction

$$T_1^{(n+1)} = T_1^{(n)} + \lambda g^{(n)} \tag{B.3}$$

where the gradient of f is given by

$$g \equiv -\delta f/\delta T_1 = D_1(T_1 \otimes T_1) + 2(D_1T_1) \otimes T_1. \tag{B.4}$$

The parameter λ is chosen so as to minimize $f\lfloor T_1^{(n+1)}\rfloor$.

The speed of convergence in this method is greatly improved by introducing conjugate gradient techniques [31].

B.2. Determination of the couple of functions $t_{11,2}$, $t_{12,1}$ (same procedure for $t_{22,1}$, $t_{12,2}$)

Note $t_{11,2}$, $t_{12,1}$ by T_2, T_3 and $\partial c_{11}/\partial\rho_2$, $\partial c_{12}/\partial\rho_1$ by C_2, C_3. The two coupled equations (9) read

$$T_2(T_3 \otimes T_3) = C_2 \tag{B.5}$$

$$T_3(T_2 \otimes T_3) = C_3. \tag{B.6}$$

The functional to minimize becomes

$$\begin{aligned} f[T_2, T_3] = {} & \frac{x_2}{2}\int [D_2(r)]^2\,\mathrm{d}\boldsymbol{r} + \frac{x_3}{2}\int [D_3(r)]^2\,\mathrm{d}\boldsymbol{r} \equiv \frac{x_2}{2}\int [C_2 - T_2(T_3 \otimes T_3)]^2\,\mathrm{d}\boldsymbol{r} \\ & + \frac{x_3}{2}\int [C_3 - T_3(T_2 \otimes T_3)]^2\,\mathrm{d}\boldsymbol{r} \end{aligned} \tag{B.7}$$

where x_2 and $x_3 = 1 - x_2$ are positive free coefficients adjusted to optimize the convergence.

The partial gradients are

$$\begin{aligned} g_2 &= -\delta f/\delta T_2 = x_2 D_2(T_3 \otimes T_3) + x_3(D_3T_3) \otimes T_3 \\ g_3 &= -\delta f/\delta T_3 = x_3 D_3(T_2 \otimes T_3) + x_3(D_3T_3) \otimes T_2 + 2x_2(D_2T_2) \otimes T_3. \end{aligned} \tag{B.8}$$

Again, the steepest-descent method, which consists in choosing

$$\begin{aligned} T_2^{(n+1)} &= T_2^{(n)} + \lambda g_2^{(n)} \\ T_3^{(n+1)} &= T_3^{(n)} + \lambda g_3^{(n)} \end{aligned} \tag{B.9}$$

with λ adjusted so as to minimize the running value of f, is coupled with powerful conjugate gradient techniques.

The procedure described above works without difficulty and in fewer than a few tens of iterations for low to moderate coupling. At higher coupling (high valences in the present study), the functions $t_{ij,k}$ differ considerably from their asymptotic forms h_{ij} and the iterative minimization procedure may be lost in unphysical local minima. This especially happens when, at some stage, the convolution products in (B.1) or in (B.5), (B.6) present zeros for some distances r where the functions C do not vanish. The incorrect reaction of the numerical process is to construct diverging functions T at these distances. In these cases, an efficient procedure consists in using careful damping in r and q spaces at each iteration, starting from strong damping and progressively releasing the constraint. This allows us to escape most of the problems and to reach a reasonable, although not perfect, convergence. The reason for this absence of perfect resolution seems to be less a possible failure of the chosen numerical integration techniques than the mathematical form of the BHP definition itself. For an *exact* determination of the $t_{ij,k}$ functions, as exact as in the resolution of the integral equation or in the bridge function calculation, a modified, less constraining version of the BHP prescription should be derived.

References

[1] Belloni L 2000 *J. Phys.: Condens. Matter* **12** R549
[2] Verwey E J W and Overbeek J Th G 1948 *Theory of Stability of Lyophobic Colloids* (Amsterdam: Elsevier)
[3] Belloni L 1998 *Colloids Surf.* A **140** 227
[4] Torrie G M and Valleau J P 1980 *J. Chem. Phys.* **73** 5807
Jönsson B, Wennerström H and Halle B 1990 *J. Phys. Chem.* **84** 2179
Megen W and Snook I 1980 *J. Chem. Phys.* **73** 4656
[5] Guldbrand L, Jönsson B, Wennerström H and Linse P 1984 *J. Chem. Phys.* **80** 2221
Valleau J P, Ivkov R and Torrie G M 1991 *J. Chem. Phys.* **95** 520
Kjellander R and Marcelja S 1984 *Chem. Phys. Lett.* **112** 49
Kjellander R and Marcelja S 1985 *J. Chem. Phys.* **82** 2122
Kjellander R and Marcelja S 1986 *J. Chem. Phys.* **90** 1230
Kjellander R 1996 *Ber. Bunsenges. Phys. Chem.* **100** 894
Kjellander R, Akesson T, Jönsson B and Marcelja S 1992 *J. Chem. Phys.* **97** 1424
[6] Linse P and Jönsson 1982 *J. Chem. Phys.* **78** 3167
[7] Vlachy V, Marshall C H and Haymet A D J 1989 *J. Am. Chem. Soc.* **111** 4160
[8] Linse P 1990 *J. Chem. Phys.* **93** 1376
[9] Delville A 1994 *Langmuir* **10** 395
[10] Hribar B, Kalyuzhnyi Y V and Vlachy V 1996 *Mol. Phys.* **87** 1317
Hribar B and Vlachy V 1997 *J. Phys. Chem.* B **101** 3457
Lobaskin V and Linse P 1998 *J. Chem. Phys.* **109** 3530
[11] Linse P and Lobaskin V 2000 *J. Chem. Phys.* **112** 3917
[12] D'Amico I and Löwen H 1997 *Physica* A **237** 25
Allahyarov E, D'Amico I and Löwen H 1998 *Phys. Rev. Lett.* **81** 1334
Wu J Z, Bratko D, Blanch H W and Prausnitz J M 1999 *J. Chem. Phys.* **111** 7084
[13] Lobaskin V, Lyubartsev A and Linse P 2001 *Phys. Rev.* E **63** 20 401(R)
Rescic J and Linse P 2001 *J. Chem. Phys.* **114** 10 131
[14] Hansen J P and McDonald I R 1986 *Theory of Simple Liquids* (London: Academic)
[15] Belloni L 1985 *Chem. Phys.* **99** 43
[16] Belloni L 1986 *Phys. Rev. Lett.* **57** 2026
[17] Belloni L 1987 *Thèse d'Etat* Paris VI
[18] Orkoulas G and Panagiotopoulos A Z 1999 *J. Chem. Phys.* **110** 1581
Belloni L 1993 *J. Chem. Phys.* **98** 8080
[19] Attard P and Miklavic S J 1993 *J. Chem. Phys.* **99** 6078
[20] Zerah H and Hansen J P 1986 *J. Chem. Phys.* **84** 2336

[21] Belloni L 1988 *J. Chem. Phys.* **88** 5143
[22] Rescic J, Vlachy V and Haymet A D J 1990 *J. Am. Chem. Soc.* **112** 3398
[23] Kalyuzhnyi Y V, Vlachy V, Holovko M F and Stell G 1995 *J. Chem. Phys.* **102** 5770
[24] Barrat J L, Hansen J P and Pastore G 1988 *Mol. Phys.* **63** 747–67
[25] Iyetomi H and Ichimaru S 1983 *Phys. Rev.* A **27** 3241
Wiechen J 1986 *J. Chem. Phys.* **85** 7364
[26] Zerah G 1985 *J. Comput. Phys.* **61** 280
[27] Barker J A and Monaghan J J 1962 *J. Chem. Phys.* **36** 2564
Haymet A D, Rice S A and Madden W G 1981 *J. Chem. Phys.* **74** 3033
Belloni L and Spalla O 1997 *J. Chem. Phys.* **107** 465
[28] Lee L L 1974 *J. Chem. Phys.* **60** 1197
Kjellander R and Sarman S 1989 *J. Chem. Phys.* **90** 2768
[29] Beresford-Smith B and Chan D Y C 1982 *Chem. Phys. Lett.* **92** 474
Senatore G and Blum L 1985 *J. Phys. Chem.* **89** 2676
Belloni L 1986 *J. Chem. Phys.* **85** 519
Khan S, Morton T L and Ronis D 1987 *Phys. Rev.* A **35** 4295
[30] Adelman S A 1976 *J. Chem. Phys.* **64** 724
[31] Press W H, Flannery B P, Teukolsky S A and Vetterling W T 1986 *Numerical Recipes* (Cambridge: Cambridge University Press)